

Tensor-Free Second-Order Differential Dynamic Programming

John N. Nganga¹ and Patrick M. Wensing¹

Abstract—This paper presents a method to reduce the computational complexity of including second-order dynamics sensitivity information into the Differential Dynamic Programming (DDP) trajectory optimization algorithm. A tensor-free approach to DDP is developed where all the necessary derivatives are computed with the same complexity as in the iterative Linear Quadratic Regulator (iLQR). Compared to linearized models used in iLQR, DDP more accurately represents the dynamics locally, but it is not often used since the second-order derivatives of the dynamics are tensorial and expensive to compute. This work shows how to avoid the need for computing the derivative tensor by instead leveraging reverse-mode accumulation of derivative information to compute a key vector-tensor product directly. We benchmark this approach for trajectory optimization with multi-link manipulators and show that the benefits of DDP can often be included without sacrificing evaluation time, and can be done in fewer iterations than iLQR.

I. INTRODUCTION

In recent years, online optimal control strategies have gained widespread interest in many applications from motion planning of robots to control of chemical processes [1]–[3]. Rather than relying on manually derived policies, these control strategies optimize a metric notion of cost that encodes desired task goals. This approach then allows online control performance that is generalizable across tasks or environments. For example, online optimization may allow a manipulator to rapidly tailor its movements to a grasped object whose weight is not known a priori, or may allow for legged systems to tailor their gaits to sensed terrains and inevitable disturbances.

However, for robots with even a few links, the underlying system dynamics are complex, nonlinear, and expensive to evaluate. These features challenge the ability to solve trajectory optimization problems online, particularly in systems with a large number of degrees of freedom (DoFs). Yet, the motivation to perform online optimization is often greater for these very systems, since a high DoF morphology gives the needed flexibility and mobility to adapt to a wider range of situations. Since the curse of dimensionality precludes the ability of exploring the full state space, online optimal control strategies often settle on exploring within a local neighborhood. Even then, the optimization of trajectories is often orders of magnitude slower than real-time. For many years, control approaches in the legged robotics literature have sidestepped this burden by employing simple models to enable faster computation [1].

Recently, whole-body trajectory optimization is becoming more feasible and has gained increased interest as com-

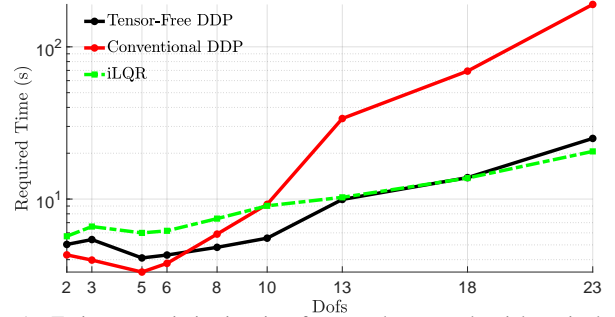


Fig. 1. Trajectory optimization time for an underactuated serial manipulator swing-up task vs. DoFs. Black curve: Proposed tensor-free second-order DDP. Red curve: Second-order DDP with explicit computation of second-order dynamics derivative tensors. Green curve: iLQR method that approximates DDP using first-order dynamics derivatives to save computation time.

putation power progresses [4]–[6]. For example, [7] used Differential Dynamic Programming DDP [8] for a humanoid to perform complex tasks such as getting up from an arbitrary pose. DDP exploits the sparsity of an optimal control problem (OCP), and its output includes an optimal trajectory along with a locally optimal feedback policy, which can be used to handle disturbances [6]. While DDP natively does not address constraints, many recent approaches using Augmented Lagrangian [9], [10], interior point [11], and relaxed barrier strategies [6], [12] have been proposed to handle general state and control constraints, with specialized approaches considered for control limit constraints [13], [14]. Other work across [15]–[18] has considered multi-threading and parallelization of the DDP algorithm to accelerate its computation. Finally, Li et al. [19] combine the advantages of whole-body DDP and simple models by sequentially considering both over the horizon. Collectively, these previous works show broad potential impact from advances to numerical methods for DDP.

Originally described in [8], DDP uses a second-order approximation of the dynamics when constructing a second-order approximation of the optimal cost-to-go. However, in practice (e.g., [4], [7], [20]) many researchers have opted to use a first-order dynamics approximation due to its faster evaluation time, giving rise to the iterative Linear Quadratic Regulator (iLQR). While the second-order dynamics information retains higher fidelity to the full model locally, it is represented by a three-dimensional tensor and is expensive to compute. Moreover, compared to vectors and matrices, tensors are more difficult to store and manipulate, and while this is not a fundamental limiter, it is a practical consideration. In this work, we alleviate these computational and practical considerations by describing a tensor-free approach to the full second-order DDP algorithm (Fig. 1).

¹Authors are with the Department of Mechanical Engineering, University of Notre Dame, Notre Dame, IN 46556, USA {jnganga, pwensing}@nd.edu

A. Specific Contributions

This work presents and combines several advances for including second-order dynamics sensitivity information into DDP. The final result is a method for computing this information with the same computational complexity as first-order dynamics derivatives (e.g., as in iLQR). The key step is the use of reverse-mode derivative accumulation to compute the second-order derivatives needed in DDP. This step enables an order reduction compared to methods that explicitly compute a derivative tensor for the dynamics. Two subsequent improvements to the approach are presented to further reduce computations. First, we show how needed second-order information related to the forward dynamics can be related to associated information from the inverse dynamics, akin to first-order results in [21], [22]. Second, we introduce a modification to the Recursive-Newton-Euler Algorithm (RNEA) that supports this process and further reduces computational demands. Fig. 1 overviews a benchmark of the proposed methods against iLQR and against DDP approaches that explicitly compute derivative tensors.

II. BACKGROUND: TRAJECTORY OPTIMIZATION

This work considers the efficient solution of a finite-horizon OCP for a rigid-body system such as an articulated robot. This section reviews background on dynamics and trajectory optimization with a focus on the DDP algorithm.

A. Dynamics

The inverse dynamics (ID) of a rigid-body system is given by

$$\boldsymbol{\tau} = \mathbf{M}(\mathbf{q})\ddot{\mathbf{q}} + \mathbf{C}(\mathbf{q}, \dot{\mathbf{q}}) + \boldsymbol{\tau}_g(\mathbf{q}) \triangleq \text{ID}(\mathbf{q}, \dot{\mathbf{q}}, \ddot{\mathbf{q}}, \mathbf{a}_g),$$

where $\mathbf{M}(\mathbf{q})$ represents the mass matrix, $\mathbf{C}(\mathbf{q}, \dot{\mathbf{q}})$ Coriolis terms, and $\boldsymbol{\tau}_g(\mathbf{q})$ the gravity term with \mathbf{a}_g the gravitational acceleration. We group the Coriolis and gravity terms together as $\mathbf{h}(\mathbf{q}, \dot{\mathbf{q}}) = \mathbf{C}(\mathbf{q}, \dot{\mathbf{q}}) + \boldsymbol{\tau}_g(\mathbf{q})$. The RNEA [23], [24] can evaluate ID with $\mathcal{O}(n)$ complexity where n is the number of DoFs in the system. The forward dynamics (FD) of the system can be formulated as

$$\ddot{\mathbf{q}} = \mathbf{M}(\mathbf{q})^{-1} (\boldsymbol{\tau} - \mathbf{h}(\mathbf{q}, \dot{\mathbf{q}})) \triangleq \text{FD}(\mathbf{q}, \dot{\mathbf{q}}, \boldsymbol{\tau}, \mathbf{a}_g).$$

When the fourth argument is omitted for ID or FD, gravity of 9.81 m/s² downward is assumed. The Articulated-Body Algorithm (ABA) [24] can compute FD in $\mathcal{O}(n)$ complexity and is an efficient alternative to $\mathcal{O}(n^3)$ algorithms that explicitly calculate and invert the mass matrix to carry out FD (e.g., [25]). Continuous trajectories for the state $\mathbf{x} = [\mathbf{q}^T, \dot{\mathbf{q}}^T]^T$ and control input $\boldsymbol{\tau}$ are discretized herein using a numerical integration scheme. While the strategies proposed are generally applicable for application with any explicit integration scheme, forward Euler integration is assumed for the remaining development such that:

$$\mathbf{x}_{k+1} = \mathbf{f}(\mathbf{x}_k, \mathbf{u}_k) \triangleq \mathbf{x}_k + h \begin{bmatrix} \dot{\mathbf{q}} \\ \text{FD}(\mathbf{q}, \dot{\mathbf{q}}, \boldsymbol{\tau}) \end{bmatrix}, \quad (1)$$

where h is the integration stepsize.

B. Differential Dynamic Programming

Herein, DDP [8] and iLQR [20] are used to solve an OCP with a cost function of the form

$$V_0(\mathbf{x}_0, \mathbf{U}_0) = \ell_f(\mathbf{x}_N) + \sum_{k=0}^{N-1} \ell_k(\mathbf{x}_k, \mathbf{u}_k) \quad (2)$$

where $\ell_k(\mathbf{x}_k, \mathbf{u}_k)$ represents the running cost, $\ell_f(\mathbf{x}_N)$ represents the terminal cost incurred at the end of a horizon, and $\mathbf{U}_0 = [\mathbf{u}_0, \mathbf{u}_1, \dots, \mathbf{u}_{N-1}]$ is the control sequence over the horizon. A cost-to-go function $V_k(\mathbf{x}_k, \mathbf{U}_k)$ can be similarly defined from any time point as the partial sum of costs from time k to N . The cost-to-go function $V_0(\mathbf{x}_0, \mathbf{U}_0)$ in (2) is minimized with respect to \mathbf{U}_0 , with states subject to the discrete system dynamics (1), providing

$$\mathbf{U}_0^*(\mathbf{x}_0) = \underset{\mathbf{U}_0}{\text{argmin}} V_0(\mathbf{x}_0, \mathbf{U}_0).$$

Throughout the paper, the star superscript refers to an optimal value. DDP optimizes over each control \mathbf{u}_i separately, working backwards in time by approximating Bellman's equation

$$V_k^*(\mathbf{x}) = \min_{\mathbf{u}_k} \left[\underbrace{\ell_k(\mathbf{x}_k, \mathbf{u}_k) + V_{k+1}^*(\mathbf{f}(\mathbf{x}_k, \mathbf{u}_k))}_{Q_k(\mathbf{x}_k, \mathbf{u}_k)} \right] \quad (3)$$

where $V_N^*(\mathbf{x}_N) = \ell_f(\mathbf{x}_N)$.

Consider a perturbation to Q_k due to small perturbations around a nominal state-control pair $\bar{\mathbf{x}}_k$ and $\bar{\mathbf{u}}_k$ such that

$$\delta Q_k(\delta \mathbf{x}_k, \delta \mathbf{u}_k) = Q_k(\bar{\mathbf{x}}_k + \delta \mathbf{x}_k, \bar{\mathbf{u}}_k + \delta \mathbf{u}_k) - Q_k(\bar{\mathbf{x}}_k, \bar{\mathbf{u}}_k).$$

Expanding the δQ -function to second order leads to

$$\delta Q_k \approx \frac{1}{2} \begin{bmatrix} 1 \\ \delta \mathbf{x}_k \\ \delta \mathbf{u}_k \end{bmatrix}^T \begin{bmatrix} 0 & Q_{\mathbf{x}}^T & Q_{\mathbf{u}}^T \\ Q_{\mathbf{x}} & Q_{\mathbf{xx}} & Q_{\mathbf{ux}}^T \\ Q_{\mathbf{u}} & Q_{\mathbf{ux}} & Q_{\mathbf{uu}} \end{bmatrix} \begin{bmatrix} 1 \\ \delta \mathbf{x}_k \\ \delta \mathbf{u}_k \end{bmatrix}. \quad (4)$$

Omitting the time index k for conciseness, these coefficients are defined as follows:

$$Q_{\mathbf{x}} = \ell_{\mathbf{x}} + \mathbf{f}_{\mathbf{x}}^T V'_{\mathbf{x}} \quad (5a)$$

$$Q_{\mathbf{u}} = \ell_{\mathbf{u}} + \mathbf{f}_{\mathbf{u}}^T V'_{\mathbf{x}} \quad (5b)$$

$$Q_{\mathbf{xx}} = \ell_{\mathbf{xx}} + \mathbf{f}_{\mathbf{x}}^T V'_{\mathbf{xx}} \mathbf{f}_{\mathbf{x}} + V'_{\mathbf{x}} \cdot \mathbf{f}_{\mathbf{xx}} \quad (5c)$$

$$Q_{\mathbf{uu}} = \ell_{\mathbf{uu}} + \mathbf{f}_{\mathbf{u}}^T V'_{\mathbf{xx}} \mathbf{f}_{\mathbf{u}} + V'_{\mathbf{x}} \cdot \mathbf{f}_{\mathbf{uu}} \quad (5d)$$

$$Q_{\mathbf{ux}} = \ell_{\mathbf{ux}} + \mathbf{f}_{\mathbf{u}}^T V'_{\mathbf{xx}} \mathbf{f}_{\mathbf{x}} + V'_{\mathbf{x}} \cdot \mathbf{f}_{\mathbf{ux}}. \quad (5e)$$

The prime in (5) denotes the next time step, i.e., $V'_{\mathbf{xx}} = V_{\mathbf{xx}}(k+1)$. The last terms in (5c - 5e) denote contraction with a tensor and are ignored in iLQR, representing the main difference between DDP and iLQR. These coefficients (5) could alternatively be viewed through derivatives of the Hamiltonian function

$$H_k(\mathbf{x}, \mathbf{u}, \boldsymbol{\lambda}) = \ell_k(\mathbf{x}, \mathbf{u}) + \boldsymbol{\lambda}^T \mathbf{f}(\mathbf{x}, \mathbf{u}), \quad (6)$$

where $\boldsymbol{\lambda}$ is a co-state vector. For example,

$$Q_{\mathbf{x}} = \nabla_{\mathbf{x}} H_k(\mathbf{x}_k, \mathbf{u}_k, V'_{\mathbf{x}}) \quad \text{and} \\ Q_{\mathbf{ux}} = \nabla_{\mathbf{ux}}^2 H_k(\mathbf{x}_k, \mathbf{u}_k, V'_{\mathbf{x}}) + \mathbf{f}_{\mathbf{u}}^T V'_{\mathbf{xx}} \mathbf{f}_{\mathbf{x}}.$$

Minimizing (4) over $\delta \mathbf{u}_k$ attains the incremental control

$$\begin{aligned} \delta \mathbf{u}_k^* &= \underset{\delta \mathbf{u}_k}{\operatorname{argmin}} \delta Q_k(\delta \mathbf{x}_k, \delta \mathbf{u}_k) \\ &= -\underbrace{Q_{\mathbf{u}\mathbf{u}}^{-1} Q_{\mathbf{u}}}_{:=\boldsymbol{\kappa}_k} - \underbrace{Q_{\mathbf{u}\mathbf{u}}^{-1} Q_{\mathbf{u}\mathbf{x}}}_{:=\mathbf{K}_k} \delta \mathbf{x}_k, \end{aligned} \quad (7)$$

where $\delta \mathbf{x} = \mathbf{x} - \bar{\mathbf{x}}$ denotes the deviation from the nominal state. When this control is substituted in (4), the quadratic approximation of the value function can be construed as

$$\text{ER}(k) = \frac{1}{2} Q_{\mathbf{u}}^T Q_{\mathbf{u}\mathbf{u}}^{-1} Q_{\mathbf{u}} + \text{ER}(k+1) \quad (8a)$$

$$V_{\mathbf{x}}(k) = Q_{\mathbf{x}} - Q_{\mathbf{u}}^T Q_{\mathbf{u}\mathbf{u}}^{-1} Q_{\mathbf{u}\mathbf{x}} \quad (8b)$$

$$V_{\mathbf{x}\mathbf{x}}(k) = Q_{\mathbf{x}\mathbf{x}} - Q_{\mathbf{x}\mathbf{u}} Q_{\mathbf{u}\mathbf{u}}^{-1} Q_{\mathbf{u}\mathbf{x}}, \quad (8c)$$

where the $\text{ER}(k)$ is the expected reduction in cost-to-go if $\delta \mathbf{x}_k = 0$ and \mathbf{U}_k were chosen optimally. This process is repeated until a value function approximation is obtained at time $k = 0$, constituting the backward sweep of DDP.

Following this backward sweep, a forward sweep proceeds by simulating the system forward in time under the incremental control policy (7), resulting in a new state-control trajectory [8]. This optimal control law (7) is typically modified by a backtracking line-search parameter, $0 < \epsilon < 1$ such that $\mathbf{u}_k = \bar{\mathbf{u}}_k + \epsilon \boldsymbol{\kappa}_k + \mathbf{K}_k \delta \mathbf{x}_k$. The line-search parameter ensures that DDP/iLQR takes steps that result in reduction of the total cost. The resulting trajectory serves as a new nominal trajectory, with the above backward and forward sweeps repeated until some convergence criteria is met.

C. DDP and iLQR: Conceptual Comparison

Many factors influence the relative performance of iLQR and DDP, with the main difference again being that the tensorial terms in (5c - 5e) are ignored in iLQR. These second-order dynamics partials $\mathbf{f}_{\mathbf{x}\mathbf{x}}$, $\mathbf{f}_{\mathbf{u}\mathbf{u}}$, and $\mathbf{f}_{\mathbf{u}\mathbf{x}}$ are ignored in both iLQR's value function approximation and its incremental control policy (7). The effect is that while DDP experiences quadratic convergence for trajectories that are sufficiently close to local optimality, iLQR only experiences super-linear convergence (i.e., it converges more slowly). However, if the running and terminal costs are strictly convex, iLQR can be simplified relative to DDP since the terms (5c - 5e) in iLQR then ensure that $Q_{\mathbf{u}\mathbf{u}}$ is always positive definite. By comparison the addition of the tensor terms (5c - 5e) in DDP can render $Q_{\mathbf{u}\mathbf{u}}$ indefinite, requiring regularization [7], [26], which incurs additional computational cost. The choice of DDP and iLQR in application then becomes a cost-benefit analysis among these differences with iLQR favored in recent work [4], [7], [20]. The derivatives of the dynamics are the most computationally expensive terms in DDP, motivating the exploration of methods for their efficient evaluation.

III. CONTRIBUTION: EFFICIENT COMPUTATION OF SECOND-ORDER DERIVATIVES FOR DDP

As noted, iLQR and DDP require first- and second-order derivatives of the dynamics respectively. Here, we concentrate on the partials of dynamics as viewed through the partials of the Hamiltonian (6) with a co-state vector

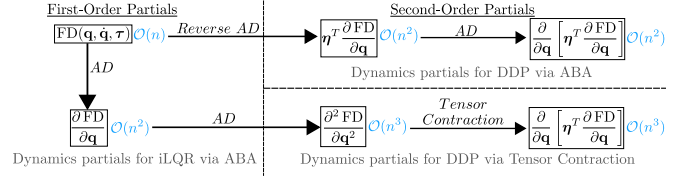


Fig. 2. Computational approach for the partials needed in iLQR via ABA, DDP via ABA, and DDP via Tensor Contraction methods

$\boldsymbol{\lambda} = [\boldsymbol{\xi}^T, \boldsymbol{\eta}^T]^T$. Using (1) and (6) the Hamiltonian can be written as

$$H_k(\mathbf{x}, \mathbf{u}, \boldsymbol{\lambda}) = \ell_k(\mathbf{x}, \mathbf{u}) + \begin{bmatrix} \boldsymbol{\xi} \\ \boldsymbol{\eta} \end{bmatrix}^T \left(\mathbf{x} + h \left[\text{FD}(\mathbf{q}, \dot{\mathbf{q}}, \boldsymbol{\tau}) \right] \right).$$

Focusing on just the second-order partials of $H_k(\mathbf{x}, \mathbf{u}, \boldsymbol{\lambda})$ with respect to \mathbf{q} , and dropping the arguments for conciseness, we note that the partials can be written as

$$\begin{aligned} \frac{\partial^2 H}{\partial q_i \partial q_j} &= \frac{\partial^2 \ell}{\partial q_i \partial q_j} + h \begin{bmatrix} \boldsymbol{\xi} \\ \boldsymbol{\eta} \end{bmatrix}^T \frac{\partial}{\partial q_i} \left(\frac{\partial}{\partial q_j} \left[\frac{\dot{\mathbf{q}}}{\text{FD}} \right] \right) \\ &= \frac{\partial^2 \ell}{\partial q_i \partial q_j} + h \boldsymbol{\eta}^T \frac{\partial}{\partial q_i} \left[\frac{\partial}{\partial q_j} \text{FD} \right] \end{aligned} \quad (9)$$

In (9), the second-order partial of FD is the most expensive term to compute. It represents a bottleneck in DDP since computing it for all possible i and j results in a tensor $\frac{\partial^2 \text{FD}}{\partial q^2}$ with n^3 elements. These elements are computed with total complexity $\mathcal{O}(n^3)$ before being contracted with $\boldsymbol{\eta}$ at an additional $\mathcal{O}(n^3)$ total cost. This conventional strategy is denoted as *DDP via Tensor Contraction*.

The key insight is that reverse mode derivative accumulation can be applied to yield an $\mathcal{O}(n^2)$ method to evaluate (9) for all i and j . This approach is diagrammed in Fig. 2 and described in Section III-A. We then review the relationship between first-order partials of ID and FD in Section III-B, and build upon them to further accelerate the calculation of second-order partials in Sections III-C and III-D.

A. Reverse Mode Accumulation to Efficiently Compute (9)

Consider a function $\mathbf{g}(\mathbf{x}) : \mathbb{R}^n \rightarrow \mathbb{R}^m$ and suppose it can be computed with complexity $\mathcal{O}(C(n, m))$, where $C(\cdot, \cdot)$ is a function of its arguments. Given any fixed vector $\boldsymbol{\gamma} \in \mathbb{R}^m$, reverse mode derivative accumulation [27] provides a standard approach to evaluate

$$\boldsymbol{\gamma}^T \frac{\partial \mathbf{g}}{\partial \mathbf{x}} = \sum_{j=1}^m \gamma_j \frac{\partial g_j}{\partial \mathbf{x}} = \frac{\partial}{\partial \mathbf{x}} [\boldsymbol{\gamma}^T \mathbf{g}] \quad (10)$$

with complexity $\mathcal{O}(C(n, m))$. Reverse-mode accumulation applies chain rule in reverse along the computational graph for a function evaluation [27], and is conceptually equivalent to the popular backpropagation algorithm [28]. This process is automated in packages that support reverse-mode auto-differentiation (AD) (e.g., CasADi [29]). The approach is powerful in the sense that while (10) appears to require all of the partials of $\mathbf{g}(\mathbf{x})$ for computation, when the matrix of partials $\frac{\partial \mathbf{g}}{\partial \mathbf{x}}$ is contracted with a vector on the left, that contraction can be computed with the same complexity as the original function $\mathbf{g}(\mathbf{x})$. This does not mean that the

evaluation of (10) and $\mathbf{g}(\mathbf{x})$ require the same number of operations. In practice, however, the cost to evaluate (10) is bounded above by a small constant times the cost to evaluate $\mathbf{g}(\mathbf{x})$, where that constant is often between three to four [27, Section 3.3].

Returning to (9), since the partials of FD are contracted with the vector $\boldsymbol{\eta}$ on the left, the desired partials can be computed efficiently using reverse mode approaches. Since FD can be calculated in $\mathcal{O}(n)$, reverse mode AD can be used to compute $\boldsymbol{\eta}^T \frac{\partial \text{FD}}{\partial \mathbf{q}}$ in $\mathcal{O}(n)$ operations as well. This result is then differentiated further, achieving the necessary result $\frac{\partial}{\partial \mathbf{q}} \left[\boldsymbol{\eta}^T \frac{\partial \text{FD}}{\partial \mathbf{q}} \right]$ in $\mathcal{O}(n^2)$ operations – the same computational complexity as the first-order partials for FD itself. When partials for DDP are obtained with this approach, we denote the method as *DDP via ABA* (see Fig. 2). The next subsection recalls methods for accelerating the calculation of first-order derivatives of the dynamics, which are then reconsidered in light of the new second-order results.

B. Revisiting First-Order Derivatives

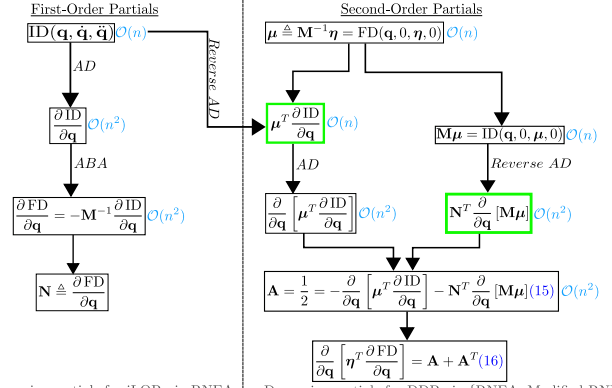
The iLQR and DDP algorithms require first-order derivatives of the dynamics, and these can be computed in $\mathcal{O}(n^2)$ operations with AD tools applied to the ABA. When dynamics derivatives are computed in this manner, the resulting iLQR algorithm is denoted as *iLQR via ABA*. The derivatives of FD are, however, related to the derivatives of ID via a simple relationship [21], [22]. For an arbitrary vector \mathbf{z} that can either represent the \mathbf{q} or $\dot{\mathbf{q}}$ vector, the first-order partials of FD can be obtained via

$$\left. \frac{\partial \text{FD}}{\partial \mathbf{z}} \right|_{\mathbf{q}_0, \dot{\mathbf{q}}_0, \boldsymbol{\tau}_0} = -\mathbf{M}^{-1}(\mathbf{q}_0) \left. \frac{\partial \text{ID}}{\partial \mathbf{z}} \right|_{\mathbf{q}_0, \dot{\mathbf{q}}_0, \boldsymbol{\tau}_0} \quad \text{and} \quad (11)$$

$$\left. \frac{\partial \text{FD}}{\partial \boldsymbol{\tau}} \right|_{\mathbf{q}_0, \dot{\mathbf{q}}_0, \boldsymbol{\tau}_0} = -\mathbf{M}^{-1}(\mathbf{q}_0) = \left(\left. \frac{\partial \text{ID}}{\partial \ddot{\mathbf{q}}} \right|_{\mathbf{q}_0, \dot{\mathbf{q}}_0, \ddot{\mathbf{q}}_0} \right)^{-1}, \quad (12)$$

where \mathbf{q}_0 , $\dot{\mathbf{q}}_0$, $\ddot{\mathbf{q}}_0$, and $\boldsymbol{\tau}_0$ refer to the point of linearization.

These relationships provide an alternate $\mathcal{O}(n^2)$ method for the first-order partials of FD. The term $\left. \frac{\partial \text{ID}}{\partial \mathbf{z}} \right|$ can be computed in $\mathcal{O}(n^2)$ complexity with AD tools or specialized algorithms (e.g., [21], [22]). The explicit computation of the mass matrix inverse can be avoided in (11) by instead applying it indirectly via calls to the ABA with the columns of $\left. \frac{\partial \text{ID}}{\partial \mathbf{z}} \right|$ used as inputs for $\boldsymbol{\tau}$. We denote this method as *iLQR via RNEA*. In state of the art implementations, however, the partials of FD are computed via (11) with $\mathcal{O}(n^3)$ complexity as follows. The partials of ID are computed with $\mathcal{O}(n^2)$ complexity, the mass matrix inverse is computed once with $\mathcal{O}(n^2)$ complexity (e.g., via [30]), and a dense matrix-matrix multiply in (11) finally sets the complexity at $\mathcal{O}(n^3)$. Since matrix-matrix multiplications are heavily optimized on modern hardware, this approach can be faster than the lower-order one. The next sections apply a similar relationship between ID and FD in the second-order case, applying reverse-mode strategies to retain $\mathcal{O}(n^2)$ computation cost.



Dynamics partials for iLQR via RNEA Dynamics partials for DDP via {RNEA, Modified RNEA}

Fig. 3. Computational approach for the partials needed in *iLQR via RNEA*, *DDP via RNEA*, and *DDP via Modified RNEA*. For *DDP via Modified RNEA*, the highlighted blocks (in green) can be accelerated using the Modified RNEA (see Algo. 1)

C. Further Improving Second-Order Partial for DDP

As the main technical contribution of the paper, this section presents an efficient way to include the second-order dynamics partials in DDP by employing reverse-mode AD and the relationship between first-order sensitivities (11). The derivation concentrates on the second-order partials, $\boldsymbol{\eta}^T \frac{\partial}{\partial q_j} \left[\frac{\partial \text{FD}}{\partial q_i} \right]$ in (9), with final results for other second-order partials summarized at the end. The approach is diagrammed in Fig. 3 as a companion to the development. The derivation makes use of the following identity

$$\frac{\partial^2 \text{ID}}{\partial q_i \partial \ddot{\mathbf{q}}} = \frac{\partial}{\partial q_i} \mathbf{M}(\mathbf{q}) = \frac{\partial \mathbf{M}}{\partial q_i} \quad (13)$$

and the fact that for a fixed \mathbf{q} , $\dot{\mathbf{q}}$, and $\boldsymbol{\tau}$, $\text{ID}(\mathbf{q}, \dot{\mathbf{q}}, \ddot{\mathbf{q}})$ is implicitly dependent on FD through composition via $\ddot{\mathbf{q}} = \text{FD}(\mathbf{q}, \dot{\mathbf{q}}, \boldsymbol{\tau})$. Therefore, the partials of ID include the partials of FD through the chain rule product of compositions. We start by using (11) and writing the second-order partials:

$$\begin{aligned} \boldsymbol{\eta}^T \frac{\partial}{\partial q_j} \left[\frac{\partial \text{FD}}{\partial q_i} \right] &= -\boldsymbol{\eta}^T \frac{\partial}{\partial q_j} \left[\mathbf{M}^{-1} \left. \frac{\partial \text{ID}}{\partial q_i} \right|_{\mathbf{q}, \dot{\mathbf{q}}, \ddot{\mathbf{q}}=\text{FD}(\mathbf{q}, \dot{\mathbf{q}}, \boldsymbol{\tau})} \right] \\ &= \boldsymbol{\eta}^T \mathbf{M}^{-1} \left[\frac{\partial \mathbf{M}}{\partial q_j} \mathbf{M}^{-1} \frac{\partial \text{ID}}{\partial q_i} - \frac{\partial^2 \text{ID}}{\partial q_i \partial q_j} - \frac{\partial^2 \text{ID}}{\partial q_i \partial \ddot{\mathbf{q}}} \frac{\partial \text{FD}}{\partial q_j} \right] \end{aligned} \quad (14)$$

whereby the last term in this result is a product of the chain-rule computation of the second-order partials of ID. The identity (13) allows for the rewrite of (14) such that

$$\begin{aligned} \boldsymbol{\eta}^T \frac{\partial}{\partial q_j} \left[\frac{\partial \text{FD}}{\partial q_i} \right] &= \boldsymbol{\eta}^T \mathbf{M}^{-1} \left[\frac{\partial \mathbf{M}}{\partial q_j} \mathbf{M}^{-1} \frac{\partial \text{ID}}{\partial q_i} - \frac{\partial^2 \text{ID}}{\partial q_i \partial q_j} - \frac{\partial \mathbf{M}}{\partial q_i} \frac{\partial \text{FD}}{\partial q_j} \right]. \end{aligned}$$

Here we recognize that the matrix-vector product $\mathbf{M}^{-1} \boldsymbol{\eta}$ is a constant term and can be computed efficiently using the ABA algorithm by ignoring gravity and the Coriolis term and using $\boldsymbol{\eta}$ as an input in place of $\boldsymbol{\tau}$. We fix that result as $\boldsymbol{\mu} \triangleq \mathbf{M}^{-1} \boldsymbol{\eta} = \text{FD}(\mathbf{q}, 0, \boldsymbol{\eta}, 0)$ (i.e., we no longer consider it as dependent on \mathbf{q} in the remainder of the development).

Further, we note that the first-order partials of the dynamics are also needed in DDP, and can be computed as in the previous subsection. We, therefore, fix each $\nu_i \triangleq \frac{\partial \text{FD}}{\partial q_i}$, and can re-use this information in the previous equation as follows

$$\begin{aligned} \eta^T \frac{\partial}{\partial q_j} \left[\frac{\partial \text{FD}}{\partial q_j} \right] \\ = -\mu^T \frac{\partial}{\partial q_j} [\mathbf{M}\nu_i] - \frac{\partial}{\partial q_j} \left[\mu^T \frac{\partial \text{ID}}{\partial q_i} \right] - \mu^T \frac{\partial}{\partial q_i} [\mathbf{M}\nu_j]. \end{aligned}$$

This equation has a unique structure in that the terms $\frac{\partial}{\partial q_i} [\mathbf{M}\nu_j]$ and $\frac{\partial}{\partial q_j} [\mathbf{M}\nu_i]$ are related by index permutation. This observation allows us to define $\mathbf{N} \triangleq \frac{\partial \text{FD}}{\partial \mathbf{q}}$ such that

$$\mu^T \frac{\partial}{\partial q_j} [\mathbf{M}\nu_i] = \left[\mathbf{N}^T \frac{\partial}{\partial \mathbf{q}} [\mathbf{M}\mu] \right]_{ij}.$$

As a result, the following definition

$$\mathbf{A} := -\frac{1}{2} \frac{\partial}{\partial \mathbf{q}} \left[\mu^T \frac{\partial \text{ID}}{\partial \mathbf{q}} \right] - \mathbf{N}^T \frac{\partial}{\partial \mathbf{q}} [\mathbf{M}\mu] \quad (15)$$

provides

$$\frac{\partial}{\partial \mathbf{q}} \left[\eta^T \frac{\partial \text{FD}}{\partial \mathbf{q}} \right] = \mathbf{A} + \mathbf{A}^T. \quad (16)$$

Both of the terms in \mathbf{A} can be computed in $\mathcal{O}(n^2)$ as follows. For the $\frac{\partial}{\partial \mathbf{q}} \left[\mu^T \frac{\partial \text{ID}}{\partial \mathbf{q}} \right]$ term, $\mu^T \frac{\partial \text{ID}}{\partial \mathbf{q}}$ can first be computed using reverse mode AD, then AD can be used again for the derivative of that result (Fig. 3). For the $\mathbf{N}^T \frac{\partial}{\partial \mathbf{q}} [\mathbf{M}\mu]$ term, we can use the RNEA algorithm to carry out $\mathbf{M}\mu = \text{ID}(\mathbf{q}, 0, \mu, 0)$ by ignoring gravity and the Coriolis terms. This calculation is an $\mathcal{O}(n)$ operation. Considering the n columns of \mathbf{N} to contract on the left of $\mathbf{N}^T \frac{\partial}{\partial \mathbf{q}} [\mathbf{M}\mu]$ provides an $\mathcal{O}(n^2)$ method via reverse mode AD. The first-order partials in \mathbf{N} have to be computed for any iLQR/DDP method, and are thus not an additional cost. Figure 3 illustrates the described approach (16). Even though the revised formulas (15), (16) result in same complexity as applying reverse-mode AD to ABA directly, the new approach gives lower computational cost since RNEA is simpler than ABA.

Formulas for the other second-order partials are as follows. Using the same approach as before, we can show that

$$\frac{\partial}{\partial \dot{\mathbf{q}}} \left[\eta^T \frac{\partial \text{FD}}{\partial \dot{\mathbf{q}}} \right] = -\frac{\partial}{\partial \dot{\mathbf{q}}} \left[\mu^T \frac{\partial \text{ID}}{\partial \dot{\mathbf{q}}} \right].$$

For the mixed partials of \mathbf{q} and $\dot{\mathbf{q}}$, we can show that

$$\frac{\partial}{\partial \mathbf{q}} \left[\eta^T \frac{\partial \text{FD}}{\partial \dot{\mathbf{q}}} \right] = -\Psi^T \frac{\partial}{\partial \mathbf{q}} [\mathbf{M}(\mathbf{q})\mu] - \frac{\partial}{\partial \mathbf{q}} \left[\mu^T \frac{\partial \text{ID}}{\partial \dot{\mathbf{q}}} \right],$$

where $\Psi = \frac{\partial \text{FD}}{\partial \dot{\mathbf{q}}}$. Finally, for the mixed partials of \mathbf{q} and τ , the resulting relationship is

$$\frac{\partial}{\partial \mathbf{q}} \left[\eta^T \frac{\partial \text{FD}}{\partial \tau} \right] = -\Xi^T \frac{\partial}{\partial \mathbf{q}} [\mathbf{M}(\mathbf{q})\mu],$$

where $\Xi = \frac{\partial \text{FD}}{\partial \tau}$. Using reverse-mode tools, all these partials can be computed with $\mathcal{O}(n^2)$ complexity. We denote DDP algorithms that use is approach as *DDP via RNEA*.

Across these derivations, the term $\mu^T \frac{\partial \text{ID}}{\partial \mathbf{q}}$ is common. For the desired term $\mu^T \frac{\partial \text{ID}}{\partial \dot{\mathbf{q}}}$ we can either (1) use reverse AD with the RNEA algorithm to calculate result or (2) provide a method to compute the term $\mu^T \text{ID}$, and then calculate its gradient with AD. While the two approaches are similar, we present a refactoring of the RNEA to reduce computation requirements for $\mu^T \text{ID}$ before applying AD.

D. Modified RNEA Algorithm

Here, we follow heavily from spatial vector algebra, notation, and body numbering conventions in [24]. Consider a poly-articulated tree-structured system of N_B rigid bodies. We denote $p(i)$ as the parent body of body i , and use the notation $j \succeq i$ to indicate when body j is after body i in the kinematic tree. Sums over pairs of related bodies can be carried out in either of the following ways:

$$\sum_{i=1}^{N_B} \sum_{j|j \succeq i} = \sum_{j=1}^{N_B} \sum_{i|i \preceq j}. \quad (17)$$

The modified RNEA output $\mu^T \text{ID}$ satisfies $\mu^T \tau = \sum_{i=1}^N \mu_i^T \tau_i$. The torque τ_i at joint i is given as

$$\tau_i = \Phi_i^T \sum_{j|j \succeq i} {}^j \mathbf{X}_i^T \mathcal{F}_j,$$

where Φ_i gives joint i 's free-modes, $\mathcal{F}_j = \mathbf{I}_j \mathbf{a}_j + (\mathbf{v}_j \times^*) \mathbf{I}_j \mathbf{v}_j$ the inertial force of body j , \mathbf{v}_j its spatial velocity, \mathbf{a}_j its spatial acceleration, and \times^* a cross product for spatial vectors [24]. The term $\mu^T \tau$ then satisfies

$$\mu^T \tau = \sum_{i=1}^{N_B} \sum_{j|j \succeq i} \mu_i^T \Phi_i^T {}^j \mathbf{X}_i^T \mathcal{F}_j.$$

The summation above is then refactored using (17) as

$$\mu^T \text{ID} = \sum_{j=1}^{N_B} \underbrace{\left[\sum_{i|i \preceq j} {}^j \mathbf{X}_i \Phi_i \mu_i \right]^T}_{:= \mathbf{w}_j} \mathcal{F}_j. \quad (18)$$

This refactoring leads to the modified RNEA algorithm (see Algo. 1). The result is that $\mu^T \text{ID}$ can be computed in a single pass rather than two passes as in RNEA. The algorithm is still an $\mathcal{O}(n)$ algorithm but leads to a simpler computation graph for reverse mode AD. Whenever this method is used in DDP, it is referred to as *DDP via Modified RNEA*. The computation workflow in this case is given as in Fig. 3, where the modified RNEA is used to accelerate the blocks highlighted in green.

E. Summary

Before proceeding to the presentation of comparative results, we briefly review the methods introduced for incorporating partials into iLQR and DDP. When only using first-order dynamics partials, we have *iLQR via ABA* and *iLQR via RNEA*. For full second-order methods, we have *DDP via ABA*, *DDP via RNEA*, and *DDP via Modified RNEA* methods, all of which are tensor-free DDP variants. Finally the conventional DDP method *DDP via Tensor Contraction*

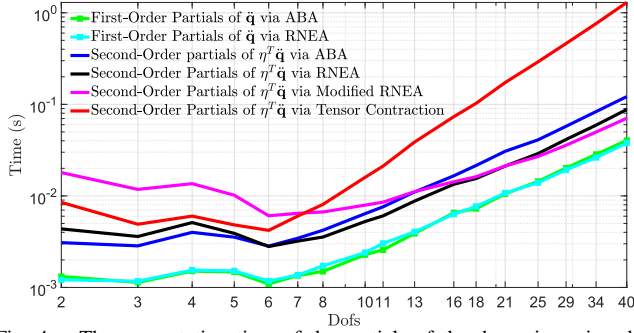


Fig. 4. The computation time of the partials of the dynamics using the aforementioned methods.

involves a computing the second-order derivative tensor. The computation approaches of these methods have been diagrammed in Fig. 2 and Fig. 3.

IV. RESULTS

To test the performance and scalability of our proposed methods, we evaluate their application to solve an OCP for an n -link pendubot. The trajectory optimization problem here was a swing-up problem and this goal was encoded via design of running and terminal costs. These costs were similar for all proposed methods regardless of the number of links in the model. As the number of links is increased, their nonlinear couplings on one another present additional challenge for solving the OCP. To further make the control problem challenging, the final link in the system was left un-actuated. For all the proposed methods, the same convergence criteria was used with convergence indicated by a negligible ($< 10^{-9}$) reduction in the cost function between iterations. We first compare the computation time of the dynamics partials (Section IV-A) using the methods described previously and then compare the addition of those partials within DDP/iLQR optimization frameworks as appropriate (see Section IV-B). This work was implemented in MATLAB alongside the CASADI [29] Toolkit which allows for rapid and efficient testing of AD approaches. Since the partials are evaluated in the CASADI virtual machine through MATLAB, the merits of the methods should be assessed via comparison between them, while future work will study improving absolute timing numbers via implementation in compiled C/C++.

Algorithm 1 Modified RNEA Algorithm

Require: $\mathbf{q}, \dot{\mathbf{q}}, \ddot{\mathbf{q}}, \boldsymbol{\mu}, model$

- 1: $\mathbf{v}_0 = 0, \mathbf{a}_0 = -\mathbf{a}_g, \mathbf{w}_0 = 0, s = 0$
 - 2: **for** $i = 1$ to N **do**
 - 3: $\mathbf{v}_i = {}^i\mathbf{X}_{p(i)} \mathbf{v}_{p(i)} + \Phi_i \dot{\mathbf{q}}_i$
 - 4: $\mathbf{w}_i = {}^i\mathbf{X}_{p(i)} \mathbf{w}_{p(i)} + \Phi_i \boldsymbol{\mu}_i$
 - 5: $\mathbf{a}_i = {}^i\mathbf{X}_{p(i)} \mathbf{a}_{p(i)} + (\mathbf{v}_i \times) \Phi_i \dot{\mathbf{q}}_i + \Phi_i \ddot{\mathbf{q}}_i$
 - 6: $s += \mathbf{w}_i^T (\mathbf{I}_i \mathbf{a}_i + (\mathbf{v}_i \times) \mathbf{I}_i \mathbf{v}_i)$
 - 7: **end for**
 - 8: **return** $s = \boldsymbol{\mu}^T \boldsymbol{\tau}$
-

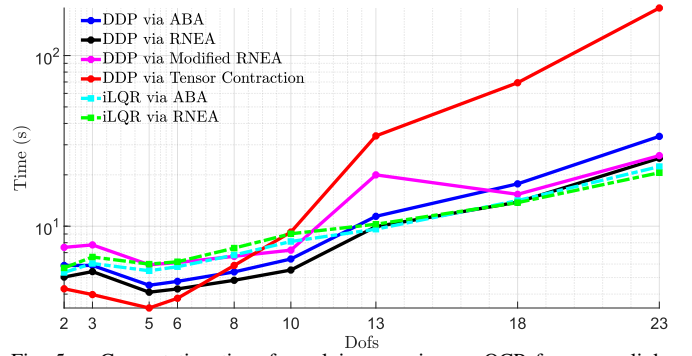


Fig. 5. Computation time for solving a swing-up OCP for an n -link pendubot.

A. Dynamics Partialals

Within DDP/iLQR, the computation of the partials of the dynamics is the most computationally expensive part of the optimization process. Figure 4 compares the computation costs of the different methods for computing these partials. As shown, evaluation of the second-order partials by tensor contraction takes the longest time whereas all other second-order partials have the same computational complexity as the first-order dynamic partials (as indicated by the slope on the log-log plot). The most competitive tensor-free second-order methods require approximately only 1.5 times more computation time than first-order partials for $n \geq 10$. Above $n = 6$, the second-order partials via RNEA/modified RNEA were faster than second-order partials via ABA since RNEA is simpler than ABA, with the modified RNEA outperforming RNEA for $n \geq 18$. These results indicate that as compared to conventional second-order tensorial dynamic partials, the proposed tensor-free methods have the potential to reduce the computational overhead of DDP to be competitive with iLQR while still retaining the convergence benefits of DDP.

B. Trajectory Optimization: DDP/iLQR Framework

We then include the dynamics partials in DDP/iLQR as appropriate and evaluate the OCP for the pendubot. Note that for an OCP with a horizon of N timesteps, each iteration of iLQR/DDP must evaluate the derivatives N times, motivating the need for their rapid evaluation. Figure 5 illustrates the time required to solve the OCP to convergence with DDP and iLQR variants. The tensor-free DDP variants had comparable evaluation time as the iLQR counterparts, while *DDP via Tensor Contraction* takes longer to optimize due to its higher-order computational complexity of evaluating dynamics derivatives.

We also evaluate the mean time to compute the DDP/iLQR variants for a 15-link pendubot model. We use a dissipative controller as the initial control trajectory and randomize the initial state vector around the ‘down’ position of the pendubot. This is a difficult problem, as it forces the control to pump energy into the system in order to drive it to the upright position. Figure 6 illustrates the time to solve the OCP with DDP/iLQR variants, whereas Fig. 7 illustrates the

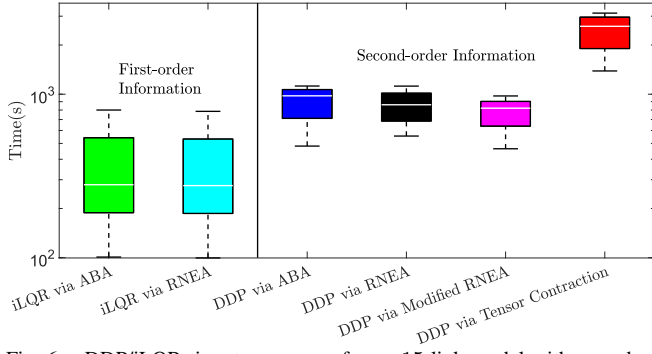


Fig. 6. DDP/iLQR time to converge for an 15-link model with a random sampling of the initial conditions around the ‘down’ position of the pendubot model

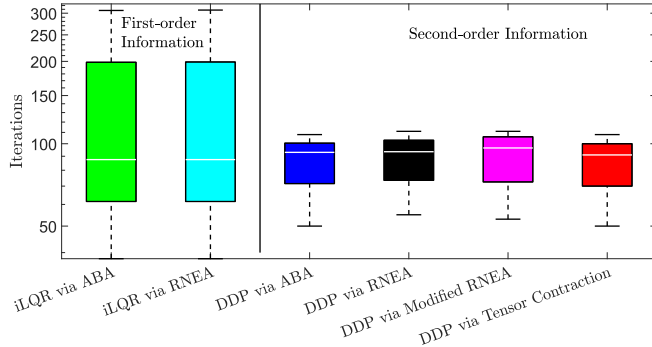


Fig. 7. DDP/iLQR number of iterations to converge for an 15-link model with a random sampling of the initial conditions around the ‘down’ position of the pendubot model

number of iterations. The DDP variants converged in fewer iterations as compared to the iLQR variants due to their quadratic convergence property. However, *DDP via Tensor Contraction* took the longest time to converge, whereas the tensor-free DDP strategies took more time compared to iLQR in this case. A portion of the additional time for DDP is attributed to repeats of the backward sweep due to the regularization needed for DDP in this case. While this motivates focus on these aspects in future work, it is worth noting that the running cost in this case was convex, and this provides benefit to iLQR in terms of avoiding regularization.

Finally, we optimize a trajectory for a 7-link lbr Kuka manipulator (available in MATLAB’s Robotic Toolbox) using DDP/iLQR methods. Figure 8 illustrates suboptimality vs. iterations for iLQR and DDP when applied to the manipulator. The suboptimality measures the difference between the current cost function value and its value at the end of the iterations. As illustrated, the DDP variants featured quadratic convergence where the iLQR variants featured super-linear convergence. This figure also illustrates that the DDP variants took fewer iterations compared to iLQR counterparts. Figure 9 illustrates the progression of that manipulator from an initial position to the balanced upright position along the optimal trajectory.

C. Discussion

As compared to conventional approaches to DDP that explicitly compute second-order derivatives of the dynamics,

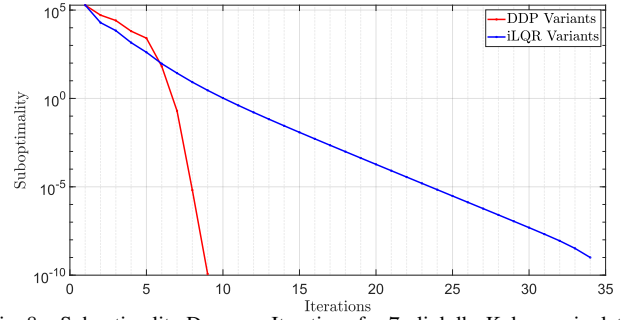


Fig. 8. Suboptimality Decay vs Iterations for 7-link lbr Kuka manipulator

tensor-free DDP variants presented here show a marked improvement in their computational complexity and computation time. This is especially important as second-order information retains better local fidelity to the original model and therefore a second-order approximation better captures the nonlinear effects of the system. This feature is expected to be important for complex systems such as quadrupeds whose coupled nonlinear dynamics might not be accurately captured by a first-order approximation. This second-order information could be of value in critical circumstances, for example, the increased fidelity could help a quadruped prevent falls or handle disturbances when traversing unstructured terrain. Succinctly, DDP’s second-order information ensures that its value function approximations and other associated approximations have a larger region of validity in state space.

We noted previously that DDP includes a regularization scheme to ensure that Q_{uu} remains positive-definite during the backward pass. This regularization incurs additional computational cost as compared to iLQR methods, and this additional cost cannot be anticipated before running the optimization. In Fig. 6, the tensor-free DDP variants needed more computation time than the iLQR variants, though we expected those evaluation times to be similar based on other tests (Fig. 1). We attribute a portion of the computational cost to repeats of the backward sweep when regularization fails, as most of the computation in DDP is spent in evaluating the backward sweep.

Lastly, our results showed that iLQR typically has more iterations but overall had comparable computation time as tensor-free DDP variants. Therefore, the benefits of DDP can be included in trajectory optimization without the previously significant sacrifice in evaluation time, and can be done in fewer iterations. This may lead to more robust model-predictive control wherein warm starting online may keep DDP iterations within the quadratic convergence well.

V. FUTURE DIRECTIONS

This work has made use of automatic differentiation tools to quickly evaluate different approaches for obtaining the derivatives needed by DDP. While these tools are convenient, they are general purpose, and thus may not be optimal. Alternative methods for taking derivatives associated with rigid-body dynamics consider the structure of the dynamics, with partials of spatial operations analytically accumulated in

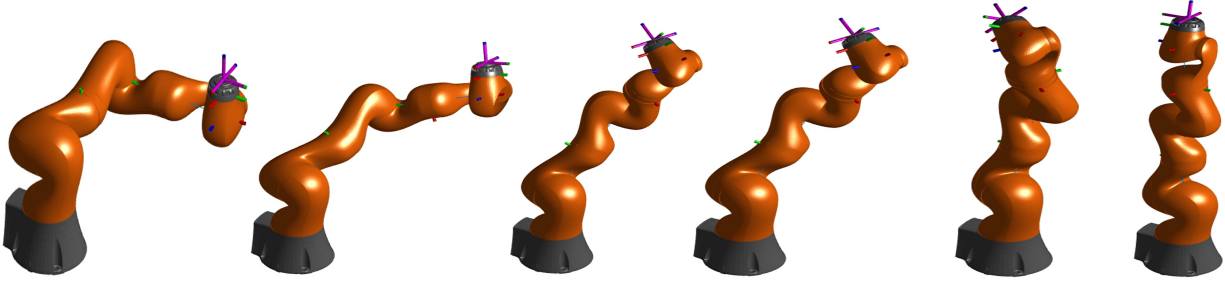


Fig. 9. Swing-up trajectory obtained by DDP/LQR for a 7-link Kuka lbr in simulation.

a recursive fashion, as done in [21], [31], [32]. The highest-performing algorithm for DDP in this paper was based on a modified RNEA algorithm that returns τ^T ID in $\mathcal{O}(n)$ complexity. Recently, we extended this algorithm with an analytical accumulation of its first-order partials in a reverse-mode fashion, and the further evaluation of this result is of immediate interest. Moreover, we aim to extend this work to address rigid-body dynamics with contacts [12], [33] by using similar methods as in this paper. This generalization would then allow for use with hybrid dynamic systems that arise in legged locomotion problems.

REFERENCES

- [1] P.-B. Wieber, R. Tedrake, and S. Kuindersma, “Modeling and control of legged robots,” in *Springer Handbook of Robotics*, 2016, pp. 1203–1234.
- [2] M. Diehl, H. J. Ferreau, and N. Haverbeke, “Efficient numerical methods for nonlinear mpc and moving horizon estimation,” in *Nonlinear model predictive control*. Springer, 2009, pp. 391–417.
- [3] D. Q. Mayne, J. B. Rawlings, C. V. Rao, and P. O. Scokaert, “Constrained model predictive control: Stability and optimality,” *Automatica*, vol. 36, no. 6, pp. 789–814, 2000.
- [4] J. Koenemann, A. Del Prete, Y. Tassa, E. Todorov, O. Stasse, M. Benezit, and N. Mansard, “Whole-body model-predictive control applied to the HRP-2 humanoid,” in *IEEE/RSJ Int. Conf. on Intelligent Robots and Systems*, 2015, pp. 3346–3351.
- [5] M. Neunert, M. Stäubli, M. Gifftthaler, C. D. Bellicoso, J. Carius, C. Gehring, M. Hutter, and J. Buchli, “Whole-body nonlinear model predictive control through contacts for quadrupeds,” *IEEE Robotics and Automation Letters*, vol. 3, no. 3, pp. 1458–1465, 2018.
- [6] R. Grandia, F. Farshidian, R. Ranftl, and M. Hutter, “Feedback mpc for torque-controlled legged robots,” in *IEEE/RSJ Int. Conf. on Intelligent Robots and Systems*, 2019, pp. 4730–4737.
- [7] Y. Tassa, T. Erez, and E. Todorov, “Synthesis and stabilization of complex behaviors through online trajectory optimization,” in *IEEE/RSJ Int. Conf. on Intelligent Robots and Systems*, 2012, pp. 4906–4913.
- [8] D. Mayne, “A second-order gradient method for determining optimal trajectories of non-linear discrete-time systems,” *International Journal of Control*, vol. 3, no. 1, pp. 85–95, 1966.
- [9] G. Lantoiné and R. P. Russell, “A hybrid differential dynamic programming algorithm for constrained optimal control problems. part 1: Theory,” *Journal of Optimization Theory and Applications*, vol. 154, no. 2, pp. 382–417, 2012.
- [10] T. A. Howell, B. E. Jackson, and Z. Manchester, “Altro: A fast solver for constrained trajectory optimization,” in *IEEE/RSJ Int. Conf. on Intelligent Robots and Systems*, 2019, pp. 7674–7679.
- [11] A. Pavlov, I. Shames, and C. Manzie, “Interior point differential dynamic programming,” *IEEE Transactions on Control Systems Technology*, 2021.
- [12] H. Li and P. M. Wensing, “Hybrid systems differential dynamic programming for whole-body motion planning of legged robots,” *IEEE Robotics and Automation Letters*, vol. 5, no. 4, pp. 5448–5455, 2020.
- [13] Y. Tassa, N. Mansard, and E. Todorov, “Control-limited differential dynamic programming,” in *IEEE Int. Conf. on Robotics and Automation*, 2014, pp. 1168–1175.
- [14] J. Marti-Saumell, J. Sola, C. Mastalli, and A. Santamaria-Navarro, “Squash-box feasibility driven differential dynamic programming,” in *IEEE/RSJ Int. Conf. on Intelligent Robots and Systems*, 2020.
- [15] E. Pellegrini and R. P. Russell, “A multiple-shooting differential dynamic programming algorithm,” in *AAS/AIAA Space Flight Mechanics Meeting*, vol. 2, 2017.
- [16] M. Gifftthaler, M. Neunert, M. Stäubli, J. Buchli, and M. Diehl, “A family of iterative gauss-newton shooting methods for nonlinear optimal control,” in *IEEE/RSJ Int. Conf. on Intelligent Robots and Systems*, 2018, pp. 1–9.
- [17] B. Plancher and S. Kuindersma, “A performance analysis of parallel differential dynamic programming on a GPU,” in *Workshop on the Algorithmic Foundations of Robotics*, 2018, pp. 656–672.
- [18] F. Farshidian, E. Jelavic, A. Satapathy, M. Gifftthaler, and J. Buchli, “Real-time motion planning of legged robots: A model predictive control approach,” in *IEEE-RAS Int. Conf. on Humanoid Robotics*, 2017, pp. 577–584.
- [19] H. Li, R. J. Frei, and P. M. Wensing, “Model hierarchy predictive control of robotic systems,” *IEEE Robotics and Automation Letters (to appear)*, 2021.
- [20] W. Li and E. Todorov, “Iterative linear quadratic regulator design for nonlinear biological movement systems,” in *ICINCO*, 2004, pp. 222–229.
- [21] J. Carpentier and N. Mansard, “Analytical derivatives of rigid body dynamics algorithms,” in *Robotics: Science and Systems*, 2018.
- [22] A. Jain and G. Rodriguez, “Linearization of manipulator dynamics using spatial operators,” *IEEE transactions on Systems, Man, and Cybernetics*, vol. 23, no. 1, pp. 239–248, 1993.
- [23] D. E. Orin, R. McGhee, M. Vukobratović, and G. Hartoch, “Kinematic and kinetic analysis of open-chain linkages utilizing newton-euler methods,” *Math Biosciences*, vol. 43, no. 1-2, pp. 107–130, 1979.
- [24] R. Featherstone, *Rigid body dynamics algorithms*. Springer, 2014.
- [25] M. W. Walker and D. E. Orin, “Efficient dynamic computer simulation of robotic mechanisms,” 1982.
- [26] L.-Z. Liao and C. A. Shoemaker, “Convergence in unconstrained discrete-time differential dynamic programming,” *IEEE Transactions on Automatic Control*, vol. 36, no. 6, pp. 692–706, 1991.
- [27] A. Grievank, “Principles and techniques of algorithmic differentiation: Evaluating derivatives,” *SIAM, Philadelphia*, 2000.
- [28] D. E. Rumelhart, G. E. Hinton, and R. J. Williams, “Learning representations by back-propagating errors,” *Nature*, vol. 323, no. 6088, pp. 533–536, 1986.
- [29] J. A. Andersson, J. Gillis, G. Horn, J. B. Rawlings, and M. Diehl, “CasADI: a software framework for nonlinear optimization and optimal control,” *Mathematical Programming Computation*, vol. 11, no. 1, pp. 1–36, 2019.
- [30] J. Carpentier, “Analytical inverse of the joint space inertia matrix,” 2018.
- [31] S.-H. Lee, J. Kim, F. C. Park, M. Kim, and J. E. Bobrow, “Newton-type algorithms for dynamics-based robot movement optimization,” *IEEE Transactions on robotics*, vol. 21, no. 4, pp. 657–667, 2005.
- [32] G. A. Sohl and J. E. Bobrow, “A recursive multibody dynamics and sensitivity algorithm for branched kinematic chains,” *J. Dyn. Sys., Meas., Control*, vol. 123, no. 3, pp. 391–399, 2001.
- [33] R. Budhiraja, J. Carpentier, C. Mastalli, and N. Mansard, “Differential dynamic programming for multi-phase rigid contact dynamics,” in *IEEE-RAS Int. Conf. on Humanoid Robots*, 2018, pp. 1–9.